





Niobium substitution suppresses the superconducting critical temperature of pressurized MoB₂

J. Lim ¹, S. Sinha ¹, A. C. Hire,^{2,3} J. S. Kim,¹ P. M. Dee ¹, R. S. Kumar,⁴ D. Popov ⁵, R. J. Hemley,⁶ R. G. Hennig,^{2,3} P. J. Hirschfeld,¹ G. R. Stewart,¹ and J. J. Hamlin¹

¹Department of Physics, University of Florida, Gainesville, Florida 32611, USA

²Department of Materials Science and Engineering, University of Florida, Gainesville, Florida 32611, USA

³Quantum Theory Project, University of Florida, Gainesville, Florida 32611, USA

⁴Department of Physics, University of Illinois Chicago, Chicago, Illinois 60607, USA

⁵HPCAT, X-ray Science Division, Argonne National Laboratory, Argonne, Illinois 60439, USA

⁶Department of Physics, Chemistry, and Earth and Environmental Sciences, University of Illinois Chicago, Chicago, Illinois 60607, USA



(Received 27 February 2023; accepted 3 August 2023; published xxxxxxxxx)

Recent study has demonstrated that MoB₂, transforming to the same structure as MgB₂ (*P6/mmm*), superconducts at temperatures above 30 K near 100 GPa [C. Pei *et al.*, *Natl. Sci. Rev.* **10**, nwad034 (2023)], and Nb substitution in MoB₂ stabilizes the *P6/mmm* structure down to ambient pressure [A. C. Hire *et al.*, *Phys. Rev. B* **106**, 174515 (2022)]. The current work explores the high-pressure superconducting behavior of Nb-substituted MoB₂ (Nb_{0.25}Mo_{0.75}B₂). High-pressure x-ray diffraction measurements show that the sample remains in the ambient pressure *P6/mmm* structure to at least 160 GPa. Electrical resistivity measurements demonstrate that from an ambient pressure *T_c* of 8 K (confirmed by specific heat to be a bulk effect), the critical temperature is suppressed to 4 K at 50 GPa, before gradually rising to 5.5 K at 170 GPa. The critical temperature at high pressure is thus significantly lower than that found in MoB₂ under pressure (30 K), revealing that Nb substitution results in a strong suppression of the superconducting critical temperature. Our calculations indeed find a reduced electron-phonon coupling in Nb_{0.25}Mo_{0.75}B₂, but do not account fully for the observed suppression, which may also arise from inhomogeneity and enhanced spin fluctuations.

DOI: [10.1103/PhysRevB.00.004500](https://doi.org/10.1103/PhysRevB.00.004500)

I. INTRODUCTION

The discovery of superconductivity at a critical temperature *T_c* = 39 K in MgB₂ [1] two decades ago sparked great interest in diborides amongst the scientific community. The superconductivity in this material is widely believed to be conventional in nature, i.e., deriving from the electron-phonon interaction. The high critical temperature has been attributed at least partly to high phonon energy scales related to the presence of low mass (light) elements and to the significant covalent character of the states near the Fermi surface [2,3].

A great deal of effort was focused on increasing the *T_c* to higher values by chemical substitution or pressure. These attempts were unsuccessful. Pressure causes a monotonic decrease in the *T_c* of MgB₂ [4,5]. Similarly, partial substitutions on the Mg or B sites invariably cause a reduction of *T_c* [6,7]. A number of structurally similar borides or borocarbides were also investigated, but none of these exhibited *T_c* values comparable to those found in MgB₂. A gradual decrease in further exploration of diboride superconductors followed. On the other hand, the search for high superconducting critical temperatures in light element compounds has been recommenced following the discovery of remarkably high-*T_c* values in pressurized hydrides [8–10].

The recent discovery of superconductivity in MoB₂ with a *T_c* reaching as high as 32 K at 110 GPa has renewed the interest in diborides [11]. However, it has been suggested that the mechanism of high *T_c* in MoB₂ is significantly different than that in MgB₂ [12]. At ambient pressure MoB₂ exists in an *R $\bar{3}m$* structure, which is nonsuperconducting at low pressure.

Above 25 GPa, however, superconductivity appears, with the highest *T_c* achieved in the *P6/mmm* phase (the same structure as MgB₂) at 110 GPa. These results led us to examine whether other diborides might also exhibit remarkably high critical temperatures at elevated pressures. In a recent paper [13], we reported that WB₂ reaches a maximum *T_c* of ~17 K at pressures near 90 GPa. Unlike MoB₂, bulk WB₂ adopts a *P6₃/mmc* structure over the entire measured pressure range to at least 145 GPa. Our findings suggested that the superconducting nature of WB₂ derives from stacking faults in a MgB₂-like structure.

An interesting question is whether the superconducting critical temperature of pressurized MoB₂ can be enhanced through chemical substitution. Our initial work in this direction has focused on examining the effects of partial Nb substitution on the Mo sites because NbB₂ occurs with *P6/mmm* structure in which MoB₂ superconducts above 30 K near 100 GPa. Recently, we showed, via density functional theory calculations, that phonon free energy stabilizes the *P6/mmm* structure relative to the *R $\bar{3}m$* structure at high temperatures across the Nb_{*x*}Mo_{1-*x*}B₂ series [14]. We were able to successfully synthesize Nb-substituted MoB₂ in the *P6/mmm* structure at ambient pressure via arc melting. The resulting compounds, Nb_{1-*x*}Mo_{*x*}B₂, where *x* = 0.1, 0.25, 0.5, 0.75, 0.9, were superconducting with Nb_{0.25}Mo_{0.75}B₂ having the highest *T_c* of 8 K in the series. Specific heat measurements on the *x* = 0.25 sample demonstrate bulk superconductivity and also showed a high upper critical field close to 7 T [14]. In the present study, we further investigate the superconductivity in

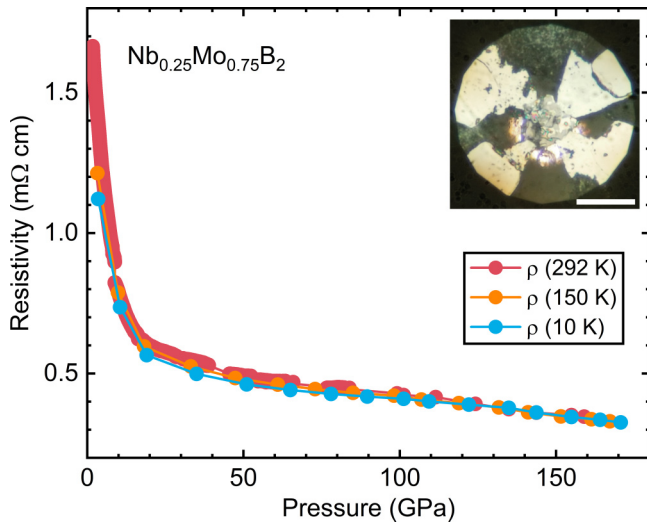


FIG. 1. Resistivity of $\text{Nb}_{0.25}\text{Mo}_{0.75}\text{B}_2$ versus pressure to 171 GPa at 10, 150, and 292 K. The resistivity curves show no noticeable change with pressure indicating the absence of any structural phase transition. Pressures at 150 K were estimated, reflecting the small changes between pressures measured at 10 and 292 K. Inset shows the microphotograph of the sample, a ruby pressure calibrant, and the four-probe method looking through the upper diamond central flat (or culet). The white scale bar indicates 50 μm .

High-pressure x-ray diffraction measurements were performed on a powdered piece of $\text{Nb}_{0.25}\text{Mo}_{0.75}\text{B}_2$ sample at beamline 16-BM-D at the Advanced Photon Source, Argonne National Laboratory. The x-ray beam had a wavelength of 0.41 \AA (30 keV) in Runs 1 and 2, which was focused to a $3 \times 4 \mu\text{m}^2$ (FWHM) spot at the sample. A MAR345 image plate detector calibrated with a CeO_2 standard was used to record the diffracted intensity with the typical exposure time of 60 to 120 seconds per image. Neon was used as the pressure medium, and pressure was determined both using an online ruby fluorescence measurement [17] up to 40 GPa as well as the equation of state of Au grains [20] loaded into the sample chamber up to 162 GPa within an error estimation of 2%. DIOPTAS [21] software was used to convert the 2D diffraction images to 1D diffraction patterns which were further analyzed by Rietveld [22] and Le Bail [23] methods using GSAS-II software [24].

To better understand the superconducting properties of $\text{Nb}_{0.25}\text{Mo}_{0.75}\text{B}_2$ under pressure we calculate the Allen-Dynes T_c at 100 GPa. The electron-phonon coupling constant λ was calculated from Eliashberg spectral function $\alpha^2F(\omega)$ obtained using the tetrahedron method as implemented in the density functional theory (DFT) code Quantum Espresso [25–27]. We use the Perdew–Burke–Ernzerhof functional for the exchange–correlation energy in the DFT calculations [28]. The virtual crystal approximation was used with the optimized norm-conserving pseudopotentials [29,30]. A k -point mesh of $20 \times 20 \times 20$ and a q -point mesh of $4 \times 4 \times 4$ were used in the calculations.

83 Nb-substituted MoB_2 ($x = 0.25$) through a combination of
84 high-pressure electrical resistivity and x-ray diffraction mea-
85 surements to pressures as high as 170 GPa.

86 II. METHODS

87 At lower pressures (< 2 GPa), we used a piston cylin-
88 der cell for resistivity measurements [15], with the
89 $\text{Nb}_{0.25}\text{Mo}_{0.75}\text{B}_2$ sample ($\sim 1.0 \times 1.0 \times 0.4 \text{ mm}^3$) mounted
90 in the van der Pauw configuration. A solution of n-
91 pentane:isoamyl alcohol (1:1 ratio) was used as the pressure
92 medium. Details on the use of the piston cylinder cell can be
93 found in Ref. [16].

94 For higher pressure resistivity measurements, a micron-
95 sized $\text{Nb}_{0.25}\text{Mo}_{0.75}\text{B}_2$ sample ($\sim 40 \times 40 \times 20 \mu\text{m}^3$) was
96 placed in a gas membrane-driven diamond anvil cell (Omni-
97 DAC from Almax-EasyLab). A ruby crystal (20 μm in
98 diameter) was used for pressure calibration [17] below
99 80 GPa. At higher pressures, the pressure was determined
100 using the Raman spectrum of the diamond anvil [18]. Pressure
101 was measured at 10 and 292 K during each cooling cycle
102 within an error estimation of 5%. Two opposing diamond
103 anvils (type Ia, 1/6-carat, 0.15 mm central flats) and a cBN-
104 epoxy, soapstone insulated Re metal gasket were used for the
105 four-probe method (see inset in Fig. 1). The diamond anvil cell
106 was then placed inside a customized continuous-flow cryo-
107 stat (Oxford Instruments). For each temperature-dependent
108 resistivity measurement, pressure was applied at room tem-
109 perature. The sample was then cooled to 1.8 K before being
110 warmed back to room temperature at a rate of $\sim 0.25 \text{ K/min}$.
111 The measurements were performed with an excitation current
112 of 0.3 mA. Further details of the nonhydrostatic high-pressure
113 resistivity techniques are given in Refs. [13,19].

143 III. RESULTS

144 The pressure-dependent resistivity curves of
145 $\text{Nb}_{0.25}\text{Mo}_{0.75}\text{B}_2$ are shown in Fig. 1 at 10, 150, and 292 K.
146 While increasing pressure at 292 K, the resistivity was
147 measured simultaneously at that temperature. However, the
148 resistivity curves at 10 and 150 K were extracted from the
149 temperature-dependent resistivity at different pressures (see
150 inset in Fig. 2). There is no significant change in resistivity
151 with respect to pressure indicating the absence of any
152 structural phase transition. We also plot the resistivity in
153 a base 10 logarithmic scale showing that the resistivity
154 smoothly decreases with pressure (see Fig. S1 in the
155 Supplemental Material [31]). The inset in Fig. 1 illustrates the
156 four-probe electrical resistivity configuration in the diamond
157 anvil cell looking through the upper diamond used in these
158 measurements.

159 Figure 2 shows selected temperature-dependent resistivity
160 curves under pressures up to 171 GPa (measured at 10 K)
161 focusing on the superconducting transition. $\text{Nb}_{0.25}\text{Mo}_{0.75}\text{B}_2$
162 superconducts at ambient pressure with a T_c of 8 K was
163 reported by our recent study [14]. Zero resistivity below
164 the superconducting transition is observed in $\text{Nb}_{0.25}\text{Mo}_{0.75}\text{B}_2$
165 throughout the whole pressure range studied. The supercon-
166 ducting transition broadens significantly above 50 GPa. We
167 denote the transition width (ΔT_c) by vertical bars in Fig. 3.
168 The resistivity curve at 171 GPa in the inset of Fig. 2 ends
169 at 200 K, where the diamonds failed during the warming
170 cycle. Nevertheless, we managed to measure the highest
171 pressure at 171 GPa using diamond anvil Raman at 10 K

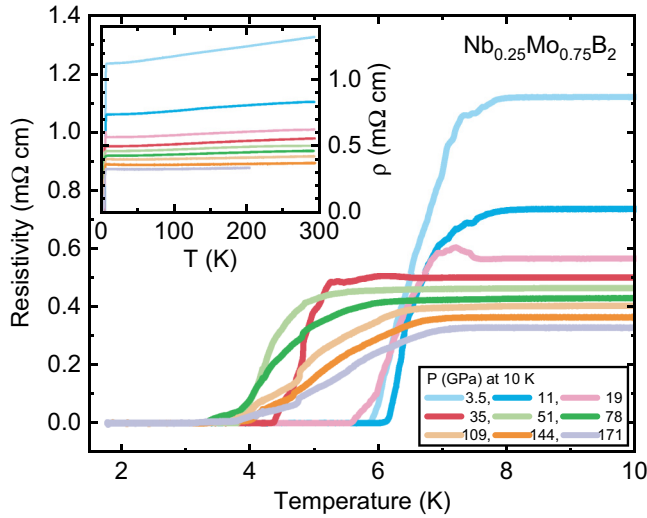


FIG. 2. Representative temperature-dependent resistivity curves of $\text{Nb}_{0.25}\text{Mo}_{0.75}\text{B}_2$ under pressure to 171 GPa (measured at 10 K) clearly showing the zero resistivity of superconducting transition between 1.8 and 10 K during each warming cycle. Inset shows the full 1.8–292 K temperature range studied.

172 during the cooling cycle (see Fig. S2 in the Supplemental
173 Material [31]).

174 The superconducting transition temperature (T_c) of
175 $\text{Nb}_{0.25}\text{Mo}_{0.75}\text{B}_2$ versus pressure to 171 GPa from Run 1 (be-
176 low 2 GPa including ambient pressure using a piston-cylinder
177 cell) and Run 2 (above 2 GPa using a diamond anvil cell) is
178 shown in Fig. 3. The $T_c(50\%)$ is defined by the temperature
179 corresponding to the 50% of normal state resistivity value just
180 above the superconducting transition (~ 10 K), whereas the

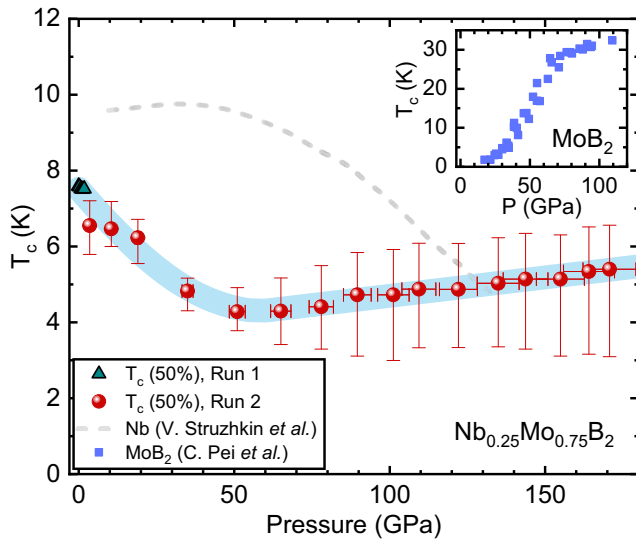


FIG. 3. Superconducting phase diagram of $\text{Nb}_{0.25}\text{Mo}_{0.75}\text{B}_2$ to 171 GPa (measured at 10 K). The superconducting transition temperature (T_c) initially goes down until ~ 50 GPa above which it monotonically increases up to 171 GPa. The upper and lower vertical bars refer to $T_c(90\%)$ and $T_c(\text{offset})$, respectively. The dashed line shows $T_c(P)$ of elemental Nb for comparison [32]. Inset refers $T_c(P)$ of pure MoB_2 from Ref. [11].

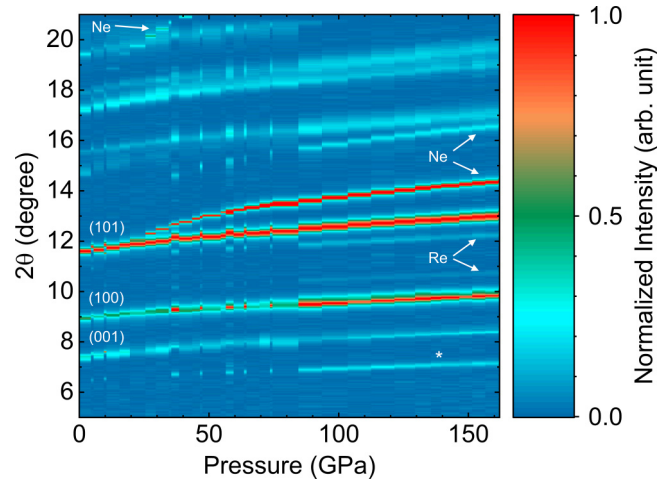


FIG. 4. Contour plot of XRD patterns of $\text{Nb}_{0.25}\text{Mo}_{0.75}\text{B}_2$ to 161 GPa at room temperature from Runs 1 and 2. The ambient structure ($P6/mmm$) persists up to the highest pressure without any structural phase transitions.

181 upper and lower vertical bars refer to the 90% and 0% (offset)
182 criteria, respectively. The pressure-dependent superconducting
183 transition temperature [$T_c(P)$] initially decreases with
184 pressure with a slope of $-0.067(6)$ K/GPa and above 50 GPa
185 monotonically increases with a slope of $0.0097(6)$ K/GPa.
186 Interestingly, the slope change in $T_c(P)$ above 50 GPa is ac-
187 companied by the significant broadening of superconducting
188 transition width (ΔT_c), defined as the difference between
189 $T_c(90\%)$ and $T_c(\text{offset})$ (see the corresponding vertical bars).
190 The nonhydrostatic condition in the measurement partially
191 contributes to the broadening due to the presence of the pres-
192 sure gradient. However, the sudden increase above 50 GPa
193 suggests the effect originates mainly from the sample itself. A
194 comparison of $T_c(P)$ between $\text{Nb}_{0.25}\text{Mo}_{0.75}\text{B}_2$ and elemental
195 Nb metal [32] is shown in Fig. 3, which clearly demonstrates
196 that the superconductivity in $\text{Nb}_{0.25}\text{Mo}_{0.75}\text{B}_2$ is not associated
197 with Nb inclusions. Previous work has demonstrated that this
198 material is a bulk superconductor [14].

199 In order to determine the presence of any structural transi-
200 tions, we have performed synchrotron x-ray diffraction (XRD)
201 measurements on powdered $\text{Nb}_{0.25}\text{Mo}_{0.75}\text{B}_2$ samples under
202 high pressure and room temperature using Ne as a pressure
203 transmitting medium in diamond anvil cells (DACs). Figure 4
204 shows a contour plot of XRD patterns whose intensities are
205 normalized with the (101) peak in Runs 1 and 2. The $P6/mmm$
206 structure at ambient pressure persists to pressures as high as
207 161 GPa as seen by the continued presence of the three
208 dominant peaks with (001), (100), and (101) Miller indices.
209 Vertically offset plots of the XRD patterns with respect to
210 pressure from Runs 1 and 2 are shown in Fig. S3 in the Supple-
211 mental Material [31]. The peaks from the highly compressible
212 Ne can be easily distinguished from those from the sample.
213 The reflections from both Ne pressure medium and Re metal
214 gasket are confirmed by their equation of state [33,34]. There
215 is a small amount of unidentified second phase between 6
216 and 7 degrees marked by a white asterisk (*). The resulting
217 pressure-volume (P - V) curve of $\text{Nb}_{0.25}\text{Mo}_{0.75}\text{B}_2$ in $P6/mmm$
218 structure at room temperature from Runs 1 and 2 is shown in

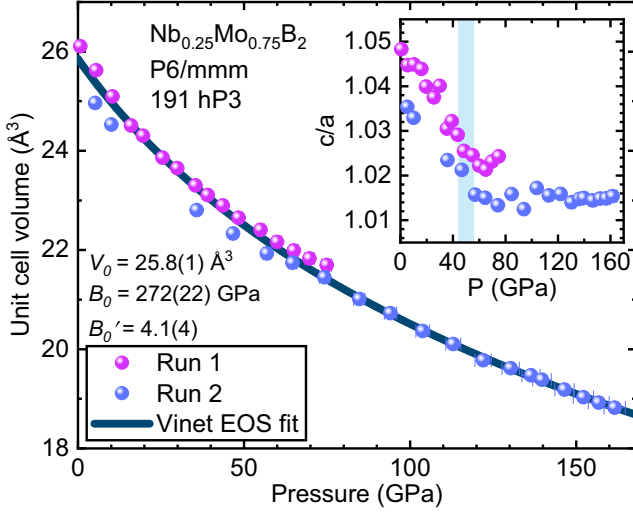


FIG. 5. P - V isotherm of $\text{Nb}_{0.25}\text{Mo}_{0.75}\text{B}_2$ to 161 GPa at room temperature. Inset shows the c/a ratio vs pressure. There is a slope change above ~ 50 GPa marked by a light blue shaded area referring to the potential correlation with the slope change of $T_c(P)$ in Fig. 3.

Fig. 5 with the c/a ratio versus pressure in the inset. There is a slope change in the c/a ratio above 50 GPa marked by a light blue shaded area, which seems to potentially correlate with the slope change in the $T_c(P)$ in Fig. 3. Interestingly, the value of the c/a ratio plateaus above 50 GPa, meaning that c lattice parameter begins to be less compressible. This may indicate that the interaction between interlayers begins to play a significant role in the $P6/mmm$ structure. The calculated a and c lattice parameters with respect to pressure are shown in Fig. S4 in the Supplemental Material [31]. The Vinet equation of state [35] is used to fit the P - V curve, which gives rise to an ambient volume 25.8 \AA^3 (V_0), bulk modulus 272 GPa (B_0), and a derivative of the bulk modulus of 4.1 (B_0'). The bulk modulus of $\text{Nb}_{0.25}\text{Mo}_{0.75}\text{B}_2$ is comparable to that of MoB_2 (296 GPa) [36].

Table III shows the computed moments of phonon frequencies, the electron-phonon coupling parameter, and the Allen-Dynes T_c (T_c^{AD}) for NbB_2 (at 0 and 100 GPa), $\text{Nb}_{0.25}\text{Mo}_{0.75}\text{B}_2$ (at 50 and 100 GPa), and MoB_2 (at 100 GPa). According to these calculations, 25% Nb substitution results in a moderate (roughly 30%) suppression of T_c compared to pure MoB_2 at 100 GPa. This occurs primarily due to a suppression of the electron-phonon coupling. Interestingly, the calculated T_c^{AD} for $\text{Nb}_{0.25}\text{Mo}_{0.75}\text{B}_2$ at both 50 and 100 GPa appear to be overestimations when compared to the experimental T_c . Contrary to the observed experimental trend, we found that T_c^{AD} decreases as the pressure increases. Note that our x-ray diffraction results indicate that at 100 GPa, $\text{Nb}_{0.25}\text{Mo}_{0.75}\text{B}_2$ and MoB_2 adopt the same $P6/mmm$ structure.

IV. DISCUSSION

One question that still follows from our experiment is why Nb-doped MoB_2 has a significantly lower transition temperatures than MoB_2 over the same pressure range studied in Ref. [11]. Much of the answer to this question can be

TABLE I. Calculated superconducting parameters. The critical temperatures, T_c were calculated using the Allen-Dynes equation with $\mu^* = 0.16$. All the calculations utilized the $P6/mmm$ structure. The DOS at the Fermi level is in units of states/eV/unit-cell volume. (* indicates calculation was performed using the experimental lattice parameters.)

Material	P (GPa)	$N(E_F)$	ω_{log} (K)	$\langle \omega^2 \rangle$ (K)	λ	T_c^{AD} (K)
NbB_2	0		354	502.6	0.75	8.86
NbB_2	100	0.795	577.1	767.4	0.48	1.65
$\text{Nb}_{0.25}\text{Mo}_{0.75}\text{B}_2$	50	1.16	268.8	426.5	1.41	23.33
$\text{Nb}_{0.25}\text{Mo}_{0.75}\text{B}_2$	100	0.99	362.2	542.7	1.02	20.14
$\text{Nb}_{0.25}\text{Mo}_{0.75}\text{B}_2^*$	100	0.90	419.8	608.3	0.94	19.58
MoB_2	100	1.14	283.3	452.5	1.48	29.17

gleaned from the literature on NbB_2 , MoB_2 , and alloyed transition metal diborides. We will focus on those findings, which are most relevant for superconductivity, starting with the density of states (DOS) near the Fermi level. When compared with NbB_2 , MoB_2 has a higher DOS near the Fermi level (Table III) and a higher fraction of electrons occupying antibonding states [37,38]. This difference helps to explain why, at ambient/low pressure, MoB_2 is a less stable diboride, preferring the trigonal $R\bar{3}m$ space group symmetry with alternating puckered boron planes instead of the hexagonal $P6/mmm$ structure realized by NbB_2 [37]. In addition, MoB_2 has a higher isotropic electron-phonon coupling constant than NbB_2 [39–43]. Here, we would like to point out that the calculated electron-phonon coupling for NbB_2 at ambient pressure of $\lambda \sim 0.43$ in Singh [44] is a result of poorly converged calculations [41,45], and our calculated value agrees with Heid *et al.* [41].

Another interesting aspect of the present study is that the experimentally realized suppression of T_c is at odds with the T_c^{AD} obtained using the Allen-Dynes formula. The theory and experiment both qualitatively agree that Nb substitution reduces the T_c in MoB_2 at high pressure (Table III) compared with MoB_2 . However, there is significant quantitative disagreement in the magnitude of T_c between the two results. Experimentally, we found that $\text{Nb}_{0.25}\text{Mo}_{0.75}\text{B}_2$ at 100 GPa exhibits only about 30% of the T_c of pure MoB_2 at the same pressure (Table III). In contrast, the Allen-Dynes equation predicts that the Nb-substituted sample should exhibit about 70% of the T_c of pure MoB_2 (i.e., for $\text{Nb}_{0.25}\text{Mo}_{0.75}\text{B}_2$, $T_c^{\text{AD}} = 19.58\text{--}20.14$ K; for MoB_2 $T_c^{\text{AD}} = 29.17$ K). In other words, the Allen-Dynes T_c^{AD} prediction works reasonably well for pure MoB_2 , but it fails to capture the strong reduction in T_c for Nb-doped MoB_2 .

Performing the same calculation for the T_c^{AD} of stoichiometric NbB_2 at ambient pressure reveals a similar overestimation. However, in that case, the degree of overestimation is difficult to gauge since the experimental literature for stoichiometric NbB_2 is rife with inconsistencies. Some papers report T_c 's between 0.62 K and 9 K [46–49], and many others report an absence of superconductivity down to the lowest temperatures measured [50–55]. There is considerably more evidence for finite T_c 's up to 8–11 K in *nonstoichiometric* NbB_2 , characterized by increasing the ratio of B to Nb

(enabled by Nb vacancies) [49–52,54–59] or decreasing this ratio via B vacancies [60,61]. Assuming that stoichiometric NbB₂ does not superconduct experimentally, except possibly at minimal temperatures, the Allen-Dynes prediction of $T_c^{AD} = 8.86$ K becomes a rather severe overestimation.

In light of the sensitivity to inhomogeneity and vacancy formation in NbB₂, we point out that MoB₂ is also susceptible to metal vacancy formation, which generally lowers the electronic density of states [43]. Taken together, we cannot rule out the role of inhomogeneities due to vacancies in the alloyed sample. Our calculations show that the tendency for metal vacancy formation in Nb_{0.25}Mo_{0.75}B₂ ($E_{vf} = 0.214$ eV) is even more likely than in NbB₂ ($E_{vf} = 1.794$ eV). The presence of vacancies on the 4d-atom site could lower the DOS at the Fermi level, reducing T_c . While we do not include these effects in our calculations of the Eliashberg function, we suspect they play a role in the discrepancy between theory and experiment.

Another potential pathology leading to T_c predictions larger than experiment could stem from spin fluctuations absent from the present formalism. Several 3d transition metals like V and Cr are better known to have significant spin fluctuations [62–66]. While Nb is generally considered a conventional electron-phonon superconductor, some claim that spin fluctuations effects are essential for estimating T_c [64,67]. We have used a modified McMillan formula defined in Eq. (2) of Ref. [68] to estimate the electron-paramagnon coupling constant required to match the experimental T_c of Nb_{0.25}Mo_{0.75}B₂ (100 GPa), obtaining $\lambda_{sf} \sim 0.15$. By comparison, to match a $T_c < 0.1$ K in NbB₂ (0 GPa) would require $\lambda_{sf} > 0.26$. These values are comparable to results for Nb in Ref. [67] and provide at least a partial explanation for the T_c mismatch. Recent theoretical study on the itinerant antiferromagnet CrB₂ suggests that spin fluctuations are suppressed under pressure, giving rise to electron-phonon-mediated superconductivity at higher pressures [66]. It is unclear if Nb_{0.25}Mo_{0.75}B₂ exhibits analogous behavior in the pressure dependence of T_c in part due to the unknown role of other effects like disorder. Further theoretical investigations are necessary to pin down the sources of the overestimation of T_c , which is outside the scope of this study.

Our measured T_c values are comparable to those reported in many other stoichiometric and nonstoichiometric ternary diboride compounds (at ambient/low pressure), such as Mo_{0.95}Sc_{0.05}B₂ ($T_c \approx 4.8$ K) [69], Mo_{0.96}Zr_{0.04}B₂ ($T_c \approx 5.9$ K) [38], Zr_{0.96}V_{0.04}B₂ ($T_c \approx 8.7$ K) [70], Zr_{0.96}Nb_{0.04}B₂ ($T_c \approx 8.1$ K) [71], relevant doped binaries such as Nb_{1-x}B₂ ($T_c \approx 9.2$ K) [51], NbB_x ($T_c \approx 9.4$ K) [47], and many other borides of Mo and Nb in the range $T_c \approx 0$ to 11.2 K [50]. There is considerably less literature studying diborides under pressures near 100 GPa, so it is not easy to draw complete comparisons with the references above.

In nonstoichiometric NbB₂, increasing the B/Nb ratio tends to expand (shrink) the c (a) lattice parameter alongside a concomitant increase in T_c [43,49–52,54–59]. This behavior indicates that a smaller spacing along the c axis is likely detrimental to superconductivity in NbB₂. Therefore, one can reasonably expect that the T_c of NbB₂ will decrease under pressure. Our T_c calculations further support this point, although the actual values are overestimates. In contrast, experiments by C. Pei *et al.* show that the T_c of MoB₂ rises

sharply with applied pressure beyond 25 GPa until a structural transition near 70 GPa, where T_c continues to increase with pressure (and the c lattice parameter keeps decreasing) but at a lower rate [11]. Hence to achieve a higher T_c value, both the materials (NbB₂ and MoB₂) take advantage of different and opposing trends in the lattice parameters. This difference possibly explains the relatively flat T_c as a function of pressure observed in our experiments. Taken together, we can see that the role of Nb in Nb_xMo_{1-x}B₂ is to increase the low-pressure stability of the AlB₂ structure ($P6/mmm$) without recreating other conditions needed for the higher T_c observed in MoB₂ under pressure.

V. CONCLUSIONS

In summary, we have studied the pressure-dependent superconducting transition temperature of Nb_{0.25}Mo_{0.75}B₂ in the same structure as MgB₂ ($P6/mmm$). Electrical resistivity measurements up to 171 GPa reveal that T_c initially decreases with increasing pressure. Above 50 GPa, T_c increases monotonically with a significant broadening of transition width ΔT_c up to the highest pressure. However, the ambient pressure T_c of 8 K is the highest T_c observed up to at least 171 GPa. Synchrotron high-pressure XRD measurements up to 161 GPa show that the slope of the c/a ratio changes above 50 GPa within the same $P6/mmm$ structure, indicating a potential correlation with the change in slope of $T_c(P)$. Our theoretical findings show a reduction of T_c , due to the weakened electron-phonon coupling, in Nb_{0.25}Mo_{0.75}B₂ compared to pure MoB₂ at high pressure, in qualitative agreement with the experiment. However, these calculations underestimate the observed suppression of T_c , suggesting that additional factors, such as inhomogeneity and spin fluctuations, may be present. High-pressure studies of other substitutions into MoB₂, which might enhance electron-phonon coupling, would be interesting to explore, to determine whether T_c values comparable to the 32 K observed in MoB₂ at 110 GPa [11] can be realized at low or ambient pressure.

ACKNOWLEDGMENTS

Work at the University of Florida was performed under the auspices of [U.S. Department of Energy Basic Energy Sciences](#) under Contract No. [DE-SC-0020385](#) and the [U.S. National Science Foundation](#), Division of Materials Research under Contract No. [NSF-DMR-2118718](#). A.C.H. and R.G.H. acknowledge additional support from the [National Science Foundation](#) under Award No. [PHY-1549132](#) (Center for Bright Beams). We thank S. Tkachev (GSECARS, University of Chicago) for sample gas loading for the x-ray diffraction measurements, and C. Kenney-Benson (HPCAT) for technical assistance. R.S.K. and R.J.H. acknowledge support from the [U.S. National Science Foundation](#) (Grants No. [DMR-2119308](#) and No. [DMR-2104881](#)). X-ray diffraction measurements were performed at HPCAT (Sector 16), Advanced Photon Source (APS), Argonne National Laboratory. HPCAT operations are supported by the DOE-National Nuclear Security Administration (NNSA) Office of Experimental Sciences. The beamtime was made possible by the Chicago/DOE Alliance Center (CDAC), which is supported by [DOE-NNSA](#) (Grant

- 413 No. DE-NA0003975). Use of the gas loading system was supported by COMPRES under NSF Cooperative Agreement 414 EAR-1606856 and by GSECARS through NSF Grant No. 415 EAR-1634415 and DOE Grant No. DE-FG02-94ER14466. 416 The Advanced Photon Source is a DOE Office of Science 417
- User Facility operated for the DOE Office of Science by Argonne National Laboratory under Contract No. DE-AC02-06CH11357. High-pressure equipment development at the University of Florida was supported by National Science Foundation CAREER Award No. DMR-1453752. 418 419 420 421 422 FQ
-
- [1] J. Nagamatsu, N. Nakagawa, T. Muranaka, Y. Zenitani, and J. Akimitsu, *Nature (London)* **410**, 63 (2001).
- [2] J. M. An and W. E. Pickett, *Phys. Rev. Lett.* **86**, 4366 (2001).
- [3] I. Mazin and V. Antropov, *Physica C: Supercond.* **385**, 49 (2003).
- [4] T. Tomita, J. J. Hamlin, J. S. Schilling, D. G. Hinks, and J. D. Jorgensen, *Phys. Rev. B* **64**, 092505 (2001).
- [5] S. Deemyad, T. Tomita, J. J. Hamlin, B. R. Beckett, J. S. Schilling, D. G. Hinks, J. D. Jorgensen, S. Lee, and S. Tajima, *Physica C: Supercond.* **385**, 105 (2003).
- [6] C. Buzea and T. Yamashita, *Supercond. Sci. Technol.* **14**, R115 (2001).
- [7] S. L. Bud'ko and P. C. Canfield, *Physica C: Supercond.* **514**, 142 (2015).
- [8] A. P. Drozdov, M. I. Erements, I. A. Troyan, V. Ksenofontov, and S. I. Shylin, *Nature (London)* **525**, 73 (2015).
- [9] M. Somayazulu, M. Ahart, A. K. Mishra, Z. M. Geballe, M. Baldini, Y. Meng, V. V. Struzhkin, and R. J. Hemley, *Phys. Rev. Lett.* **122**, 027001 (2019).
- [10] I. Osmond, O. Moulding, S. Cross, T. Muramatsu, A. Brooks, O. Lord, T. Fedotenko, J. Buhot, and S. Friedemann, *Phys. Rev. B* **105**, L220502 (2022).
- [11] C. Pei, J. Zhang, Q. Wang, Y. Zhao, L. Gao, C. Gong, S. Tian, R. Luo, M. Li, W. Yang *et al.*, *Natl. Sci. Rev.* **10**, nwad034 (2023).
- [12] Y. Quan, K.-W. Lee, and W. E. Pickett, *Phys. Rev. B* **104**, 224504 (2021).
- [13] J. Lim, A. C. Hire, Y. Quan, J. S. Kim, S. R. Xie, S. Sinha, R. S. Kumar, D. Popov, C. Park, R. J. Hemley *et al.*, *Nat. Commun.* **13**, 7901 (2022).
- [14] A. C. Hire, S. Sinha, J. Lim, J. S. Kim, P. M. Dee, L. Fanfarillo, J. J. Hamlin, R. G. Hennig, P. J. Hirschfeld, and G. R. Stewart, *Phys. Rev. B* **106**, 174515 (2022).
- [15] D. VanGennep, S. Maiti, D. Graf, S. W. Tozer, C. Martin, H. Berger, D. L. Maslov, and J. J. Hamlin, *J. Phys.: Condens. Matter* **26**, 342202 (2014).
- [16] I. R. Walker, *Rev. Sci. Instrum.* **70**, 3402 (1999).
- [17] A. D. Chijioke, W. J. Nellis, A. Soldatov, and I. F. Silvera, *J. Appl. Phys.* **98**, 114905 (2005).
- [18] Y. Akahama and H. Kawamura, *J. Appl. Phys.* **100**, 043516 (2006).
- [19] T. Matsuoka and K. Shimizu, *Nature (London)* **458**, 186 (2009).
- [20] Y. Fei, A. Ricolleau, M. Frank, K. Mibe, G. Shen, and V. Prakapenka, *Proc. Natl. Acad. Sci. USA* **104**, 9182 (2007).
- [21] C. Prescher and V. B. Prakapenka, *High Press. Res.* **35**, 223 (2015).
- [22] H. M. Rietveld, *J. Appl. Crystallogr.* **2**, 65 (1969).
- [23] A. Le Bail, H. Duroy, and J. Fourquet, *Mater. Res. Bull.* **23**, 447 (1988).
- [24] B. H. Toby and R. B. Von Dreele, *J. Appl. Crystallogr.* **46**, 544 (2013).
- [25] P. Giannozzi, S. Baroni, N. Bonini, M. Calandra, R. Car, C. Cavazzoni, D. Ceresoli, G. L. Chiarotti, M. Cococcioni, I. Dabo *et al.*, and *J. Phys.: Condens. Matter* **21**, 395502 (2009).
- [26] P. Giannozzi, O. Baseggio, P. Bonfà, D. Brunato, R. Car, I. Carnimeo, C. Cavazzoni, S. de Gironcoli, P. Delugas, F. Ferrari Ruffino *et al.*, *J. Chem. Phys.* **152**, 154105 (2020).
- [27] P. Giannozzi, O. Andreussi, T. Brumme, O. Bunau, M. B. Nardelli, M. Calandra, R. Car, C. Cavazzoni, D. Ceresoli, M. Cococcioni *et al.*, and *J. Phys.: Condens. Matter* **29**, 465901 (2017).
- [28] J. P. Perdew, K. Burke, and M. Ernzerhof, *Phys. Rev. Lett.* **77**, 3865 (1996).
- [29] D. R. Hamann, *Phys. Rev. B* **88**, 085117 (2013).
- [30] M. Schlipf and F. Gygi, *Comput. Phys. Commun.* **196**, 36 (2015).
- [31] See Supplemental Material at <http://link.aps.org/supplemental/10.1103/PhysRevB.xx.xxxxxx> for extended figures and experimental details, such as electrical resistivity (log scale), pressure determination (Raman, sample P vs membrane P), x-ray diffraction patterns (stacked up), and calculated a and c lattice parameters (up to 162 GPa), respectively
- [32] V. V. Struzhkin, Y. A. Timofeev, R. J. Hemley, and H.-k. Mao, *Phys. Rev. Lett.* **79**, 4262 (1997).
- [33] A. Dewaele, F. Datchi, P. Loubeyre, and M. Mezouar, *Phys. Rev. B* **77**, 094106 (2008).
- [34] S. Anzellini, A. Dewaele, F. Occelli, P. Loubeyre, and M. Mezouar, *J. Appl. Phys.* **115**, 043511 (2014).
- [35] P. Vinet, J. Ferrante, J. H. Rose, and J. R. Smith, *J. Geophys. Res.* **92**, 9319 (1987).
- [36] S. Yin, D. He, C. Xu, W. Wang, H. Wang, L. Li, L. Zhang, F. Liu, P. Liu, Z. Wang, C. Meng, and W. Zhu, *High Press. Res.* **33**, 409 (2013).
- [37] P. Vajeeston, P. Ravindran, C. Ravi, and R. Asokamani, *Phys. Rev. B* **63**, 045115 (2001).
- [38] L. Muzzy, M. Avdeev, G. Lawes, M. Haas, H. Zandbergen, A. Ramirez, J. Jorgensen, and R. Cava, *Physica C: Superconductivity* **382**, 153 (2002).
- [39] T. Oguchi, *J. Phys. Soc. Jpn.* **71**, 1495 (2002).
- [40] Yu. G. Naidyuk, O. E. Kvitnitskaya, I. K. Yanson, S.-L. Drechsler, G. Behr, and S. Otani, *Phys. Rev. B* **66**, 140301(R) (2002).
- [41] R. Heid, B. Renker, H. Schober, P. Adelman, D. Ernst, and K.-P. Bohnen, *Phys. Rev. B* **67**, 180510(R) (2003).
- [42] I. R. Shein, N. I. Medvedeva, and A. L. Ivanovskii, *Phys. Solid State* **45**, 1617 (2003).
- [43] I. R. Shein and A. L. Ivanovskii, *Phys. Rev. B* **73**, 144108 (2006).
- [44] P. P. Singh, *Solid State Commun.* **125**, 323 (2003).
- [45] P. P. Singh, *Phys. Rev. B* **67**, 132511 (2003).
- [46] L. Leyarovska and E. Leyarovski, *J. Less-Common Met.* **67**, 249 (1979).

- [47] J. E. Schirber, D. L. Overmyer, B. Morosin, E. L. Venturini, R. Baughman, D. Emin, H. Klesnar, and T. Aselage, *Phys. Rev. B* **45**, 10787 (1992).
- [48] H. Kotegawa, K. Ishida, Y. Kitaoka, T. Muranaka, N. Nakagawa, H. Takagiwa, and J. Akimitsu, *Physica C: Superconductivity* **378-381**, 25 (2002).
- [49] H. Takeya, K. Togano, Y. S. Sung, T. Mochiku, and K. Hirata, *Physica C: Superconductivity* **408-410**, 144 (2004).
- [50] A. S. Cooper, E. Corenzwit, L. D. Longinotti, B. T. Matthias, and W. H. Zachariasen, *Proc. Natl. Acad. Sci. USA* **67**, 313 (1970).
- [51] A. Yamamoto, C. Takao, T. Masui, M. Izumi, and S. Tajima, *Physica C: Supercond.* **383**, 197 (2002).
- [52] R. Escamilla and L. Huerta, *Supercond. Sci. Technol.* **19**, 623 (2006).
- [53] H. X. Geng, G. C. Che, W. W. Huang, S. L. Jia, H. Chen, and Z. X. Zhao, *Supercond. Sci. Technol.* **20**, 452 (2007).
- [54] E. Regalado and R. Escamilla, *J. Phys.: Condens. Matter* **19**, 376209 (2007).
- [55] M. Mudgel, V. Awana, G. Bhalla, and H. Kishan, *Solid State Commun.* **147**, 439 (2008).
- [56] V. A. Gasparov, N. S. Sidorov, I. I. Zver'kova, and M. P. Kulakov, *J. Exp. Theor. Phys. Lett.* **73**, 532 (2001).
- [57] R. Escamilla, O. Lovera, T. Akachi, A. Durán, R. Falconi, F. Morales, and R. Escudero, *J. Phys.: Condens. Matter* **16**, 5979 (2004).
- [58] C. A. Nunes, D. Kaczorowski, P. Rogl, M. R. Baldissera, P. A. Suzuki, G. C. Coelho, A. Grytsiv, G. André, F. Boureé, and S. Okada, *Acta Mater.* **53**, 3679 (2005).
- [59] T. Takahashi, S. Kawamata, S. Noguchi, and T. Ishida, *Physica C: Supercond.* **426-431**, 478 (2005).
- [60] J. K. Hulm and B. T. Matthias, *Phys. Rev.* **82**, 273 (1951).
- [61] W. T. Ziegler and R. A. Young, *Phys. Rev.* **90**, 115 (1953).
- [62] J. Castaing, P. Costa, M. Heritier, and P. Lederer, *J. Phys. Chem. Solids* **33**, 533 (1972).
- [63] A. Bauer, A. Regnat, C. G. F. Blum, S. Gottlieb-Schönmeier, B. Pedersen, M. Meven, S. Wurmehl, J. Kuneš, and C. Pfeleiderer, *Phys. Rev. B* **90**, 064414 (2014).
- [64] K. Tsutsumi, Y. Hizume, M. Kawamura, R. Akashi, and S. Tsuneyuki, *Phys. Rev. B* **102**, 214515 (2020).
- [65] C. Pei, P. Yang, C. Gong, Q. Wang, Y. Zhao, L. Gao, K. Chen, Q. Yin, S. Tian, C. Li, W. Cao, H. Lei, J. Cheng, and Y. Qi, *arXiv:2109.15213*.
- [66] S. Biswas, A. Kreisel, A. Valadkhani, M. Dürrnagel, T. Schwemmer, R. Thomale, R. Valentí, and I. I. Mazin, *Phys. Rev. B* **108**, L020501 (2023).
- [67] S. K. Bose, *J. Phys.: Condens. Matter* **21**, 025602(R) (2009).
- [68] I. I. Mazin, D. A. Papaconstantopoulos, and M. J. Mehl, *Phys. Rev. B* **65**, 100511(R) (2002).
- [69] W. Yang, G. Xiao, Q. Zhu, Y. Cui, S. Song, G.-H. Cao, and Z. Ren, *Ceram. Int.* **48**, 19971 (2022).
- [70] S. T. Renosto, H. Consoline, C. A. M. dos Santos, J. Albino Aguiar, S.-G. Jung, J. Vanacken, V. V. Moshchalkov, Z. Fisk, and A. J. S. Machado, *Phys. Rev. B* **87**, 174502 (2013).
- [71] M. D. R. Marques, F. S. Portela, L. T. Corredor, G. Zhang, J. Vanacken, V. V. Moshchalkov, L. E. Correa, S. T. Renosto, O. Cigarroa, A. J. S. Machado, and J. A. Aguiar, *Supercond. Sci. Technol.* **29**, 095007 (2016).